Mott Physics in Organic Conductors with Triangular Lattices

Kazushi Kanoda

Department of Applied Physics, University of Tokyo, Bunkyo-ku, Tokyo 113-8656, Japan; email: kanoda@ap.t.u-tokyo.ac.jp

Reizo Kato

Condensed Molecular Materials Laboratory, RIKEN, Saitama 351-0198, Japan; email: reizo@riken.jp

Annu. Rev. Condens. Matter Phys. 2011. 2:167–88

First published online as a Review in Advance on January 12, 2011

The *Annual Review of Condensed Matter Physics* is online at conmatphys.annualreviews.org

This article's doi: 10.1146/annurev-conmatphys-062910-140521

1947-5454/11/0310-0167$20.00

Keywords

organic materials, Mott transition, critical phenomena, quasi-triangular lattice, spin liquid

Abstract

Electron correlation and spin frustration are among the central issues in condensed matter physics, and their interplay is expected to bring about exotic phases with both charge and spin fluctuations. Molecular materials are playgrounds suitable for this study. Fundamentals in physics of Mott transition and spin frustration on triangular lattices are seen in the organic materials ET and $Pd(dmit)_2$ compounds. We review the experimental studies on the criticality of Mott transition with a continuously controllable pressure technique and on the ground state of the quasi-triangular-lattice Mott insulator. Mott criticality is well characterized in both charge and spin channels with unconventional critical exponents of possibly quantum nature. The ground state of the triangular-lattice Mott insulator is changed from antiferromagnet to spin liquid as the triangular lattice becomes more isotropic. The various experiments probing the nature of spin liquid are described in the light of proposed mechanisms.

1. INTRODUCTION

Mutual interaction between electrons is a source that affords various kinds of exotic electronic phases. In the absence of interaction, electrons propagate freely (but following Fermi-Dirac statistics) as Bloch waves on a periodic lattice in solid state. They gain more quantum mechanical kinetic energy, *W*, characterized by electronic bandwidth, compared with the localized state. In the presence of interaction, however, the free motion of electrons would cost the Coulomb repulsive energy when they approach each other. Assuming a simple situation of one electron per lattice site forming a half-filled band, the Coulomb repulsive energy of two electrons accommodated by a site, which is called on-site Coulomb energy *U*, represents the correlation energy. For $W >> U$, electrons keep behaving like Bloch waves with the double occupation allowed, and they are metallic. For $W << U$, however, each electron manages to avoid the double occupation and stay at each site, as with particles rather than waves. This is an insulator. Therefore, it is expected that a dramatic metal-insulator transition occurs when W and U are comparable. This is called the Mott transition, which is an interaction-induced imbalance of the electron's dual (wave and particle) nature. The interaction effect is not only restricted to the charge degrees of freedom, but it also gives various emergent phenomena in spin degrees of freedom. Even in the Mott insulator, spins, which are remaining degrees of freedom, mutually interact and can form a variety of organizations strongly depending on the lattice geometry, some of which are argued to give nontrivial organization with quantum fluctuations highly enhanced.

Organic conductors are suitable for the research of electron correlation in several respects. First, the electronic band structure, which gives a basis for considering the physics of the electronic system, is simple and clear because the system is well described by the tight-binding model of molecular orbitals. Second, owing to a rich variation in molecular arrangements, one can pursue the lattice geometry-property relation in a systematic way. Third, the van der Waals nature of molecular packing allows the precise control of the transfer integrals, namely bandwidth *W*, relative to the Coulomb repulsive energy by chemical substitution or physical pressure. In reality, the molecular conductors exhibit a variety of ground states, depending on dimensionality, lattice topology, band filling, nature, and strength of electron-electron and electron-phonon couplings (1–3).

This review is devoted to two issues in the physics of correlated electrons, namely Mott transition and the spin states of Mott insulators, which were revealed in layered organic systems. The Mott transition has long been studied since Mott's discussion on the insulating state of NiO_2 (4) and is now recognized as a key concept for understanding various emergent phenomena such as high-T_c superconductivity and colossal magnetoresistance (5). However, the critical characteristics, which tells us what the nature of phase transition is, remained unknown (**Figure 1*a***). In the Mott-insulating state, spins are usually ordered at low temperatures but can take nontrivial states on triangular lattices where geometrical frustration against antiparallel configuration makes the quantum fluctuation remarkable (**Figure 1*b***). The quantum spin liquid on triangular lattices proposed theoretically by Anderson (6) was of keen interest among the possible spin states (7–9) and long anticipated in real materials. The underlying concept is the singlet formation of spins (valence bond). The spin liquid is postulated as the quantum-mechanically fluctuating rearrangement of the singlet pairs called resonating valence bonds, whereas its order is another possible state called a valence bond solid (VBS).

These charge and spin issues were illuminated by two kinds of organic materials based on an electron donor molecule ET or an electron acceptor molecule $Pd(dmit)_2$, where ET is bis(ethylenedithio)tetrathiafulvalene and dmit is 1,3-dithiole-2-thione-4,5-dithiolate (**Figure 2**)

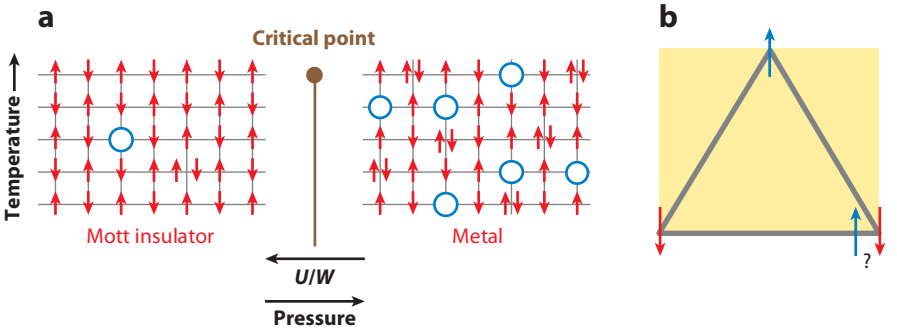

Figure 1

Two issues discussed in this article. (*a*) Conceptual phase diagram of Mott transition. In a region of $U/W > 1$ (at low pressures), the majority of particles (electrons or holes) are localized at lattice sites, whereas for $U/W < 1$ the particles can move with double occupancies and vacancies allowed. The transition between the two regimes occurs as a metal-insulator transition without symmetry breaking. Its criticality is in question. (*b*) Nontrivial spin states in geometrically frustrated lattice. Antiferromagnetically interacting spins on triangular lattices have difficulty in having an ordered ground state. Spins possibly remain disordered in the ground state in the quantum-mechanical sense. It is a long-standing question whether the spin liquid state can be realized and what its nature is.

(10, 11). They are both effectively half-filled band systems with anisotropic triangular lattices. By pressure, we can access the critical region of the Mott transition (**Figure 1*a***). The triangular feature of the molecular lattice provides an opportunity to tackle the problem of the spin frustration. Below, we present the experimental observations of Mott criticality in ET salts and spin liquid in ET and $Pd(dmit)_2$ salts.

2. κ-$(ET)_2X$

2.1. Crystal and Electronic Structures of κ-$(ET)_2X$

The ET molecule provides many 2:1 compounds, $(ET)_2X$, with various kinds of anion, X. Among them, the materials that we deal with in this section are κ-$(ET)_2X$. They are layered materials composed of conducting ET layers with 1/2 hole per ET and insulating X layers,

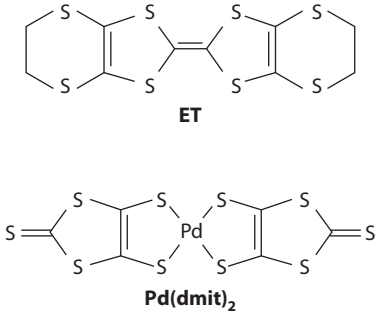

Figure 2

Two molecules that provide compounds discussed in this review. BEDT-TTF (ET) is an electron donor and gives salts $(ET)_2X$ with monovalent anion X^{-1}. $Pd(dmit)_2$ is an electron acceptor and gives salts $A[Pd(dmit)_2]_2$ with monovalent cation, A^{+1}.

as shown in **Figure 3*a***. The monovalent anion, X^{-1}, has no contribution to electronic conduction or magnetism. In the conducting layer, the ET molecules form dimers, which are arranged in a checkerboard-like pattern (**Figure 3*b***). From the band structure point of view, two ET highest occupied molecular orbitals (HOMOs) in a dimer are energetically split into bonding and antibonding orbitals, each of which forms a conduction band due to the interdimer transfer integrals (12). The two bands are well separated so that the relevant band to the hole filling is the antibonding band, which is half-filled with one hole accommodated by one antibonding orbital. The dimer arrangement is modeled to an isosceles-triangular lattice characterized by two interdimer transfer integrals, t and t' (**Figure 3*c***) of the order of 50 meV, whose anisotropy, t'/t, depends on the anion X.

2.2. Criticality of Mott Transition in ET Compounds

The competition of kinetic energy and correlation energy, which are characterized by bandwidth W and on-site Coulomb energy U, gives rise to Mott transition between wave-like itinerant electrons and particle-like localized electrons. Because the Mott transition is a metal-insulator transition without symmetry breaking, the first-order transition expected at low temperatures can have a critical endpoint at a finite temperature, as in the gas-liquid transition (**Figure 1*a***). This feature of the Mott phase diagram was first deduced by the reduction of Hubbard Hamiltonian to the so-called Blume-Emery-Griffiths model (13) and then extensively discussed in terms of dynamical mean field theory (DMFT) (14), which showed that the Mott transition belongs to the Ising universality class (15). It is well established that the κ-$(ET)_2X$ family is situated in the vicinity of Mott transition (9, 16–24). To explore the phase diagram beyond the conceptual one, and to uncover the critical behavior of Mott transition, experiments on a single material under precisely controlled pressure and temperature are required.

The compound studied is κ-$(ET)_2Cu[N(CN)_2]Cl$, which is a Mott insulator (25) with a sizable anisotropy of triangular lattices; the t'/t value is 0.75 or 0.44, according to the tight-binding calculation of molecular orbital or first-principles calculation (26), respectively. The resistivity measurements of κ-$(ET)_2Cu[N(CN)_2]Cl$ under continuously controllable He-gas pressure unveiled the Mott phase diagram (27–30), where the first-order transition line dividing the insulating and metallic phases has an endpoint around 40 K (**Figure 4**). The presence of the critical endpoint was proved in spin and lattice degrees of freedom as well; namely, nuclear magnetic resonance (NMR) (31), ultrasonic velocity (32, 33), and expansivity (34). The bending shape of the phase boundary reflects the entropy difference between the insulating

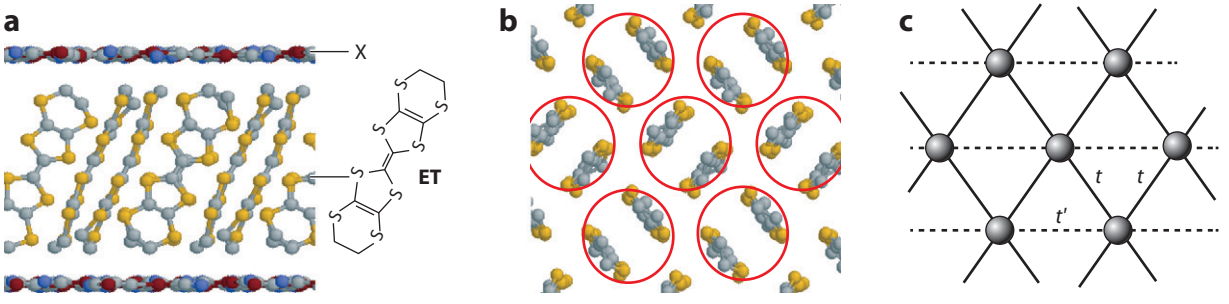

Figure 3

Structure of κ-$(ET)_2X$. (*a*) Side and (*b*) top view of the layer and (*c*) modeling the in-plane structure into an isosceles-triangular lattice with two kinds of transfer integrals.

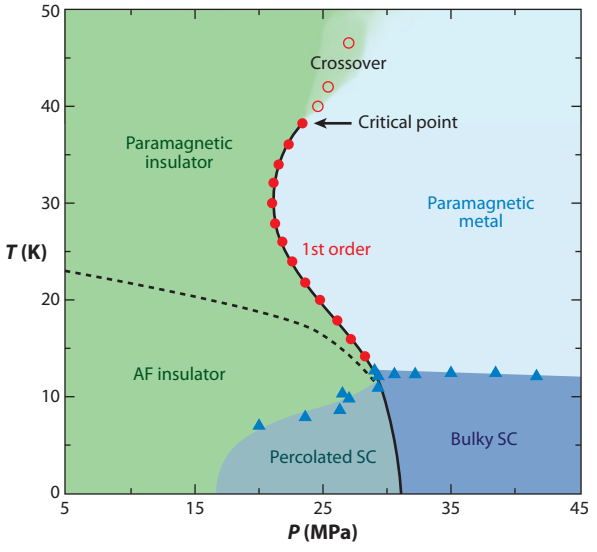

Figure 4

Pressure-temperature phase diagram of κ-$(ET)_2Cu[N(CN)_2]Cl$ determined by conductivity measurements. Abbreviations: AF, antiferromagnet; SC superconductor.

and metallic phases, according to the Clausius-Clapeiron relation; positive (negative) dT/dP at high (low) temperatures indicates that the entropy of the Mott-insulating phase is larger (smaller) than that of the metallic phase. The temperature variation of dT/dP is explained by a rapid decrease in the spin entropy of the insulating phase due to short-range order compared with the metallic phase with temperature decreased (28, 29). Therefore, the profile of the phase boundary is affected by the spin frustration, as demonstrated by cluster-DMFT studies of the Hubbard model (35–37). Although antiferromagnetic ordering and superconductivity occur at low temperatures, the critical point is far from such symmetry-breaking transitions. The critical phenomena, which are direct clues to identifying the universality class, appear around the endpoint, as is well known in the liquid-gas transition. The order parameter characterizing criticality is density in the gas-liquid transition and magnetization in the ferromagnetic transition. Mott transition can be viewed as a liquid-gas transition of double occupancies and vacancies (13), as depicted in **Figure 1*a***. In this picture, their densities are expected to play a role of order parameter and can be probed by conductivity.

Figure 5*a* shows the detailed conductance behavior under isothermal pressure sweeps in the vicinity of the critical point (38). At lower temperatures, the conductance exhibits a clear jump at a well-defined pressure, indicating the first-order metal-insulator transition. A small but finite hysteresis, which cannot be resolved in the scale of the figure, is found. At elevated temperatures, the jump is gradually diminished and vanishes at a critical endpoint, T_c, of 39.7 K. Above T_c, the conductance varies continuously against pressure, pointing to a metal-insulator crossover. The crossover pressure is defined by the pressure giving a maximum in the pressure derivative of conductance, $G'(P,T) \equiv \partial G(P,T)/\partial P$ (**Figure 5*b***). The first-order transition line and the crossover line are represented in **Figure 4** (29, 30). According to DMFT (14, 15), the order parameter of the Mott transition has a scalar nature and is measured by the conductance deviation from the value at the critical point in the metallic region, $G–G_c$ (39, 40), which was successfully demonstrated by an experiment on V_2O_3 (41). In this context, the

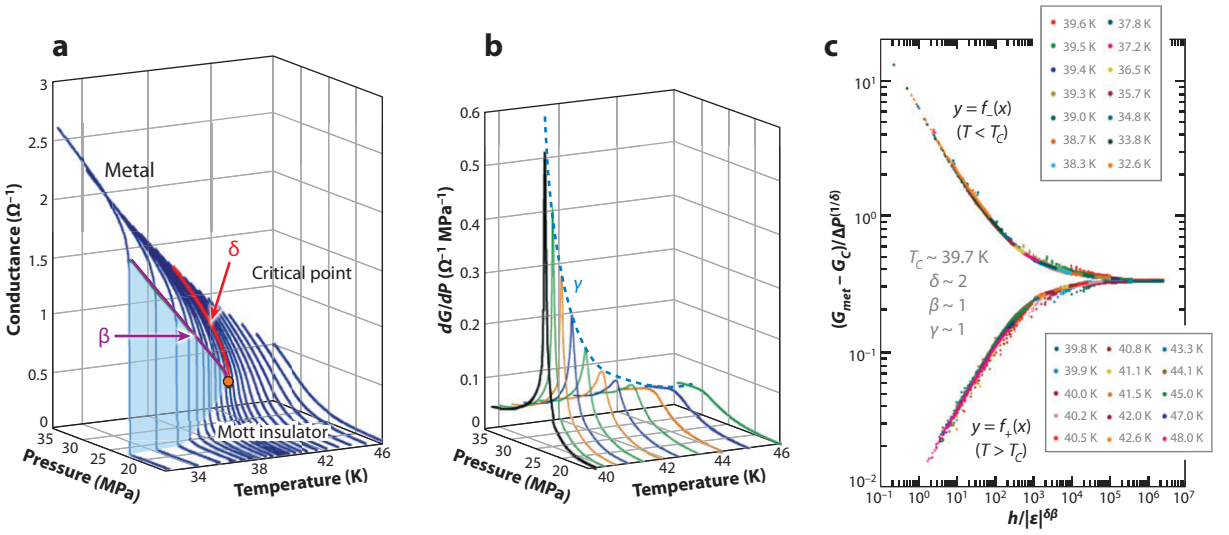

Figure 5

(*a*) Conductance, $G(P, T)$, around the critical endpoint for κ-$(ET)_2Cu[N(CN)_2]Cl$. The light blue shaded area indicates the conductance jump. The red and purple lines represent the critical behavior that gives the critical exponents δ and β, respectively. (*b*) Pressure derivative of conductance, $\partial G_T(P)/\partial P$, as a function of pressure at temperatures above the critical endpoint. The dashed blue curve represents the critical divergence of the values on the crossover line. This gives the critical exponent, γ. (*c*) Scaling plot of the whole data set of $G(P,T)$ in the metallic region. ΔP is the pressure distance to the first-order line ($T < T_c$) or the crossover line ($T > T_c$). $\Delta\varepsilon$ is the temperature distance to the critical point. ΔG is the conductance difference from the critical value, G_c, ($T < T_c$) or the crossover value, $G(P_{cross}(T))$, for $T < T_c$.

temperature dependence of $G–G_c$ along the first-order line represented in **Figure 5*a*** (purple curve) gives the critical exponent β of the conductance jump expressed by $G_{met}(T)-G_c \sim (T_c-T)^{\beta}$. The pressure dependence of $G–G_c$ at T_c (red curve) gives the exponent δ in the form $G_T(P)-G_c \sim (P-P_c)^{1/\delta}$. Moreover, the critical exponent of the spin susceptibility equivalence is extracted from the temperature dependence of the pressure derivative of conductance, $\partial G_T(P)/\partial P|_{P\,=\,P\mathrm{cross}(T)} \sim (T-T_c)^{-\gamma}$ along the crossover line (blue dashed line in **Figure 5*b***).

The experimental data are well fitted to the power-law dependence with the exponents $(\delta, \beta, \gamma) \sim (2, 1, 1)$. These values are not among established universality classes and are unconventional in the sense that the widely known universality classes have in common the features of $\delta \geq 3$ and $\beta \leq 0.5$ [(3, 0.5) are the mean-field values]. However, the (2, 1, 1) satisfies the scaling relation, $\delta = 1 + \gamma/\beta$, and another scaling prerequisite that the temperature and pressure variation of order parameter should be in a universal form of the equation of states (39, 42), which follows in the present case:

$$\{G_T(P) - G_T(P_{cross})\}/(P - P_{cross})^{1/\delta} = f_+\left(\frac{P - P_{cross}}{|T - T_c|^{\delta\beta}}\right) \text{ for } T > T_c, \qquad 1.$$

$$\{G_T(P) - G_C\}/(P - P_I)^{1/\delta} = f_-\left(\frac{P - P_I}{|T - T_C|^{\delta\beta}}\right) \text{ for } T < T_c, \qquad 2.$$

where P_{cross} and P_I represent crossover pressure above T_c and transition pressure below T_c. Using the present value, $(\delta, \beta) \sim (2, 1)$, and the whole data set of $G_T(P)$ in the metallic region

[$P > P_I$ for $T < T_c$ and $P > P_{cross}$ for $T > T_c$], we plotted in **Figure 5*c*** $\{G_T(P)-G_T(P_{cross})\}/(P-P_{cross})^{1/\delta}$ versus $(P-P_{cross})/|T-T_c|^{\delta\beta}$ for $T > T_c$, and $\{G_T(P)-G_c\}/(P-P_I)^{1/\delta}$ versus $(P-P_I)/|T-T_c|^{\delta\beta}$ for $T < T_c$. All the data fall into the two universal curves over a wide range. The successful scaling behavior supports the present analysis on the basis of the assumption that the conductance serves as the Mott order parameter.

Mott transition is a phenomenon occurring in the charge degrees of freedom due to the Coulomb interaction. How another degree of freedom of electron, namely spin whose fluctuations are ubiquitous in strongly correlated electrons, behave in the critical region is an interesting question. The NMR probes electron spins, whose fluctuations are measured by the nuclear spin-lattice relaxation rate, $1/T_1$. **Figure 6** shows the pressure dependence of the relaxation rate divided by temperature, $1/T_1T$, measured under continuously controlled He-gas pressure at several temperatures (43). A clear jump in $1/T_1T$ is emergent on the Mott transition at low temperatures; however, the jump vanishes around the critical point, followed by smooth crossover at higher temperatures. With pressure increased so as to pass through the critical point, a steep enhancement of conductance at the critical pressure is accompanied by a steep suppression of spin fluctuations (**Figure 7*a***). Mott criticality obviously manifests itself in magnetism as well as in charge transport. Note that this magnetic criticality appears as a critical change in paramagnetic spin fluctuations, not as a precursor to magnetic ordering. The detailed analysis of the data shows that $\Delta 1/T_1(P)T$ [$= 1/T_1(P)T - 1/T_1(P_c)T$] is well fitted to a power form of $|P-P_c|^{1/\delta}$ with nearly the same critical exponent of $\delta = 2$ as observed in conductance (**Figure 7*b***). Why does the Mott criticality show up in the spin degrees of freedom? The doubly occupied sites and empty sites (**Figure 1*a***) serve as charge carriers and at the same time act as spin vacancies. Therefore, the increase in conductivity and the suppression in spin fluctuations go parallel with an identical exponent reflecting the critical change in the density of doubly occupied and empty sites, which is the order parameter of the Mott transition.

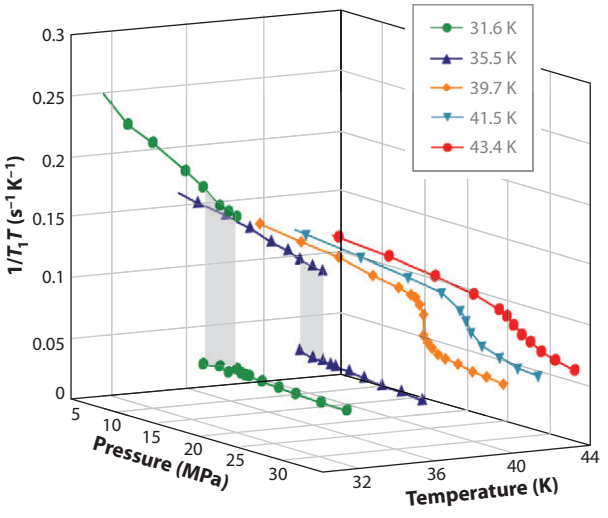

Figure 6

^{13}C NMR relaxation rate around the Mott critical endpoint. The pressure dependence of $1/T_1T$ at various temperatures. The gray shaded areas represent the coexistence of insulating and bad metallic phases. Abbreviation: NMR, nuclear magnetic resonance.

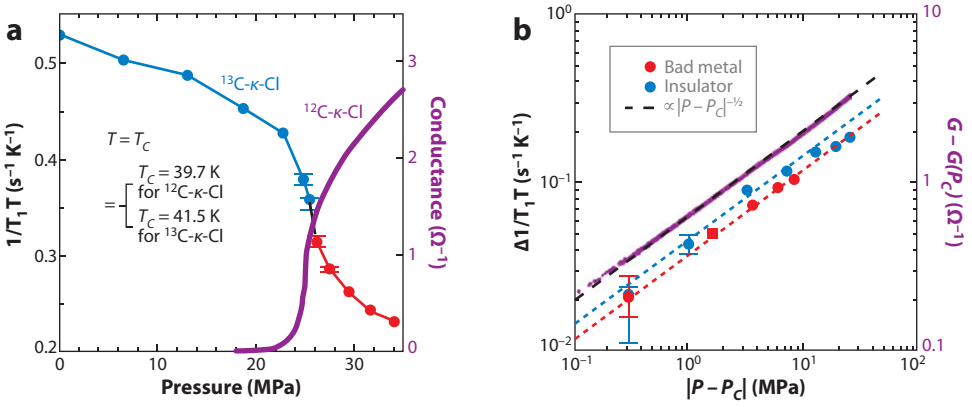

Figure 7

(*a*) Pressure dependence of ^{13}C NMR relaxation rate (*blue* and *red circles*) and conductance (*purple curve*) at the critical temperature. (*b*) Logarithmic plot of $1/T_1T$ and conductance measured from the endpoint against $|P - P_c|$. The dashed black line indicates the pressure dependence of $|P - P_c|^{1/2}$. Regarding the plot of conductance, the data above P_c are used. Abbreviation: NMR, nuclear magnetic resonance.

The next issue is how to understand these unconventional critical exponents. Imada and coworkers theoretically considered the Mott criticality in three different cases of classical (finite T_c), quantum ($T_c = 0$), and marginally quantum (in between) regimes, and showed that the exponents in the marginally quantum case are $(\delta, \beta, \gamma) = (2, 1, 1)$, which are the experimental values (44, 45). Because the present T_c is as low as 40 K, much less than 450 K in the V_2O_3, but finite, the marginal quantum criticality, if any, should cross over to the classical Ising-like one in close vicinity (probably inaccessible in the present experiments) to the finite-temperature critical point, as demonstrated numerically (45). Another scenario is proposed by Papanikolaou et al., who argued that the conductance exponents (2, 1, 1) are a consequence of nonlinear relation between the conductance, $\Delta G = G - G_c$, and Mott order parameter (46). Assuming a power relation between them, they reproduced the (2, 1, 1) with the Ising-type of order parameter. It is of interest whether this scenario explains the same exponent ($\delta = 2$) in a spin channel probed by NMR.

As a different probe, expansivity is reported to exhibit an enhancement near the Mott critical point in an analog, deuterated κ-$(ET)_2Cu[N(CN)_2]Br$ (34), and is analyzed in two ways. Assuming that expansivity is proportional to specific heat (Gruneisen law), the data turn out to point to an anomalous criticality different from the (2, 1, 1) and any known universalities (34). Assuming that the system volume is linear to the Mott order parameter, instead, the data can be consistent with the Ising universality (47). The controversy above is attributed to the problem of identifying what the Mott order parameter is and how it is probed experimentally. A consensus on the nature of Mott criticality has yet to be seen.

2.3. Antiferromagnetic Ordering Versus Spin Liquid in ET Compounds

The material κ-$(ET)_2Cu[N(CN)_2]Cl$ referred to above has anisotropy $t'/t = 0.75$ (0.44) in triangular lattices, according to quantum chemical (first-principles) calculations (26), and has an antiferromagnetic ground state in the Mott-insulating phase (25). Another Mott insulator, κ-$(ET)_2Cu_2(CN)_3$, is intriguing because the dimer triangular lattice is so close to the equilateral one [i.e., $t'/t = 1.06$ (49) or 0.80 to 0.83 (26, 49)] that the spins are more frustrated and can be

a real candidate of the quantum liquid state, which has been sought since Anderson's proposal more than 35 years ago (6). **Figure 8*a*** shows the temperature dependence of the magnetic susceptibility with the core diamagnetism subtracted (50). In contrast with the magnetic transition at 27 K in κ-$(ET)_2Cu[N(CN)_2]Cl$ as evidenced by an anomaly, κ-$(ET)_2Cu_2(CN)_3$ has no anomaly down to the lowest temperature measured, 2 K, but does have a broad peak, which is well fitted to the triangular-lattice Heisenberg model with an exchange interaction of $J \sim 250$ K (50, 51). The χ_{spin} behavior of κ-$(ET)_2Cu[N(CN)_2]Cl$ is unlikely fitted to the Heisenberg model, even if the anisotropy is considered, possibly because it is situated very close to the Mott transition, where the Hubbard model or higher-order corrections in the Heisenberg model should work.

The magnetism is further probed by NMR measurements. **Figure 8*b*** shows the single-crystal ^1H NMR spectra for κ-$(ET)_2Cu[N(CN)_2]Cl$ and κ-$(ET)_2Cu_2(CN)_3$ under the magnetic field applied perpendicular to the conducting layer (50). The line shape at high temperatures comes from the nuclear dipole interaction sensitive to the field direction against molecular orientation, which is different between the two systems. κ-$(ET)_2Cu[N(CN)_2]Cl$ shows a clear line splitting below 27 K, indicating a commensurate aniferromagnetic ordering, whose moment is estimated at 0.45 μ_B per an ET dimer by separate ^{13}C NMR studies (25, 52, 53). However, the spectra of κ-$(ET)_2Cu_2(CN)_3$ show neither distinct broadening nor splitting, which indicates the absence of long-range magnetic ordering at least down to 32 mK, 4 orders of magnitude lower than

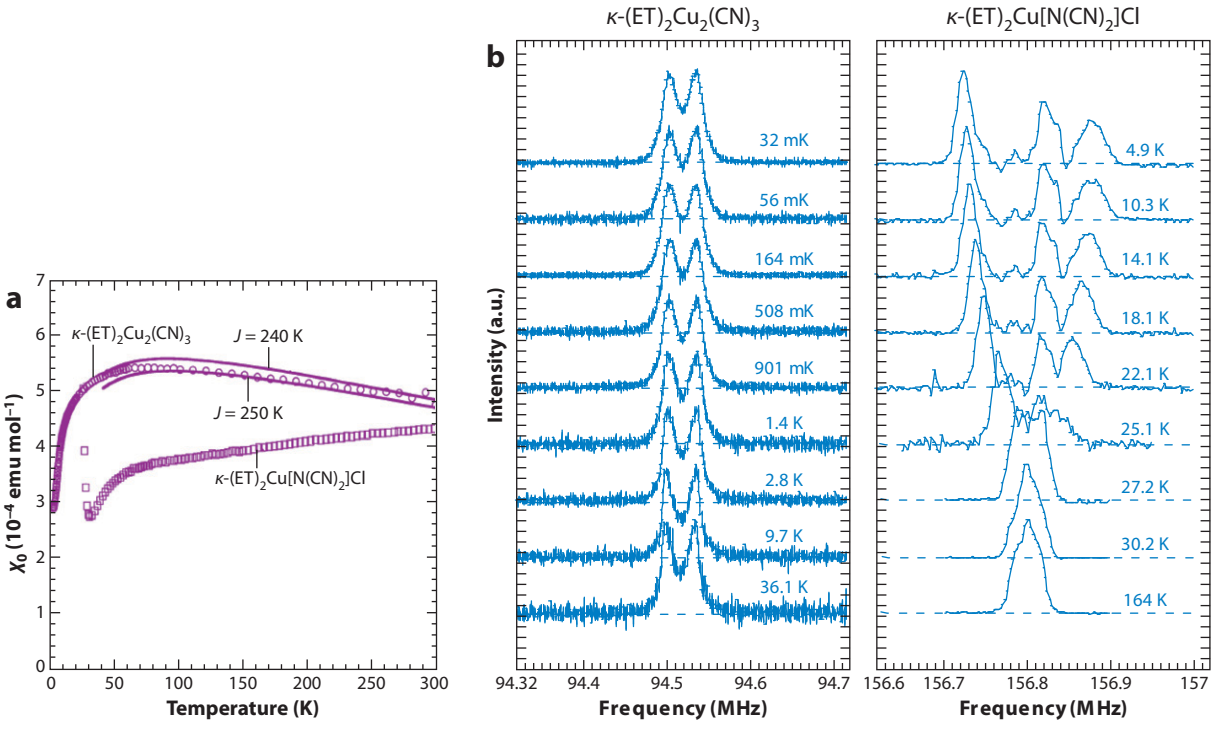

Figure 8

(*a*) Temperature dependences of spin susceptibilities of κ-$(ET)_2Cu_2(CN)_3$ and κ-$(ET)_2Cu[N(CN)_2]Cl$. The solid lines represent the results of the series expansion of the triangular-lattice Heisenberg model using [7,7] Pade approximation with $J = 240$ K and 250 K. (*b*) ^1H NMR spectra of single crystals of κ-$(ET)_2Cu_2(CN)_3$ (*left panel*) and κ-$(ET)_2Cu[N(CN)_2]Cl$ (*right panel*) under magnetic fields applied perpendicular to the conducting layer. Abbreviation: NMR, nuclear magnetic resonance.

the J value of 250 K. The result points to the realization of a quantum spin liquid in κ-$(ET)_2Cu_2(CN)_3$ due to the strong spin frustration on the nearly equilateral triangular lattice.

Theoretically, it is believed that the ground state of the triangular-lattice Heisenberg model is the 120° spirally ordered state (54). This model is appropriate for strongly correlated Mott insulators. However, the present systems are in the intermediately correlated regime because they undergo Mott transition to metals under low pressures. In this context, the Hubbard model (55–66), the Heisenberg model with higher-order exchange or ring exchange interactions (67–71), or related models (72–75) have been investigated extensively to seek possible spin liquid states without magnetic ordering. Most of them indicated the presence of quantum-disordered states. Thus, the moderate correlation, as well as the spin frustration, is key to the realization of the quantum spin liquid.

The nature of spin liquid in κ-$(ET)_2Cu_2(CN)_3$ was further studied by ^{13}C NMR (76), specific heat (77), thermal conductivity (78), and expansivity (79) measurements. Common to these quantities is an anomaly around 5–6 K. **Figures 9*a*** and ***b*** show ^{13}C NMR relaxation rate and specific heat at low temperatures, respectively. Below 8 K, $1/T_1$ decreases more steeply and C/T starts to increase, followed by a kink and a peak around 5 to 6 K, respectively, and a sharp peak in expansivity (not shown). This means that the anomaly is thermodynamic and involves at least the spin degrees of freedom. This anomaly is accompanied by NMR spectral broadening, whose field dependence indicates that the broadening is not due to a spontaneous spin ordering but rather to a field-induced inhomogeneous staggered moment. This can be caused by impurities or a Dzyaloshinsky-Moriya interaction. Whatever the origin is, that the broadening is enhanced below 5–6 K implies some change or possible symmetry breaking in the underlying

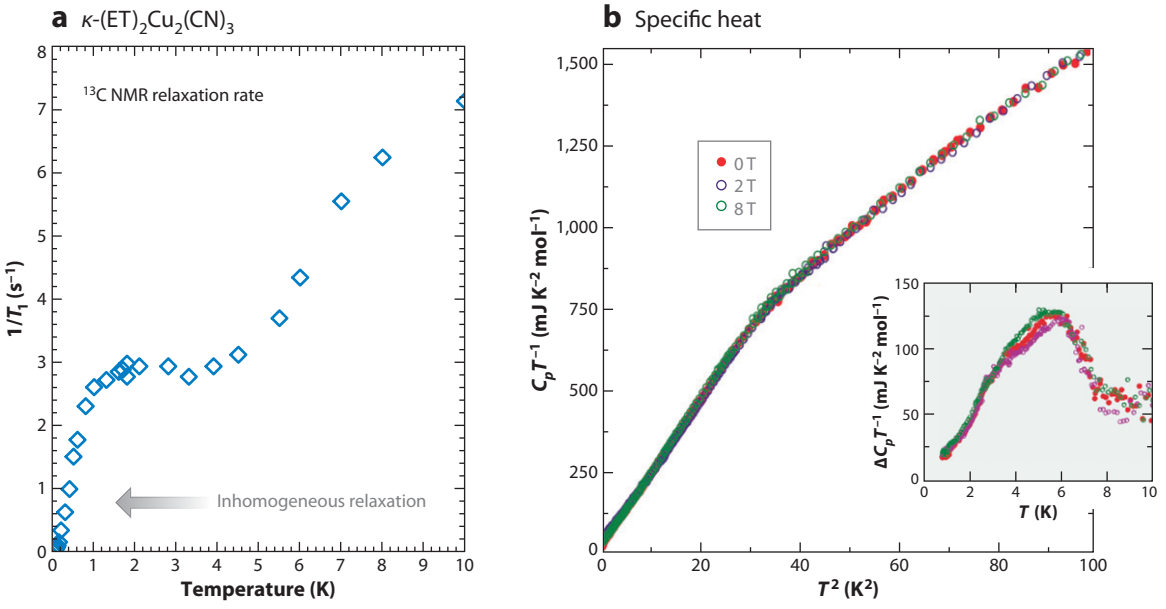

Figure 9

(*a*) ^{13}C NMR relaxation rate of κ-$(ET)_2Cu_2(CN)_3$. The nuclear relaxation becomes inhomogeneous at lower temperatures, as depicted by the graded arrow. (*b*) Specific heat divided by temperature, $C_p\,T^{-1}$, as a function of T^2 for κ-$(ET)_2Cu_2(CN)_3$ under magnetic fields of 0 T (*red*), 2 T (*purple*), and 8 T (*green*). The inset shows the difference of the heat capacities of κ-$(ET)_2Cu_2(CN)_3$ and κ-$(ET)_2Cu(NCS)_2$, which is considered to serve as a reference of phonon background. Abbreviation: NMR, nuclear magnetic resonance.

spin liquid state. The theoretical proposals such as an order of scalar chirality (67), paired spinon states (58, 59, 71, 80, 81), and Z_2 vortex transition (82) are among the possible mechanisms of the 5–6 K anomaly. Although a steep decrease in $1/T_1$ is observed well below 1 K, there appears no appreciable anomaly in specific heat and thermal conductivity around the corresponding temperatures.

A key issue on the nature of spin liquid is whether the spin liquid is gapped. The experimental observations are, however, totally controversial at present. The specific heat points to the presence of a finite γ value comparable to that in the metallic phase down to at least 0.3–0.4 K, below which the nuclear Schottky contribution becomes overwhelming (77). The thermal conductivity measurements indicate that the thermal excitation is gapped by 0.46 K (78). The ^{13}C NMR relaxation rate shows a power-law temperature dependence with an exponent of 3/2; although, the nuclear relaxation is inhomogeneous at low temperatures (76). They are all inconsistent with each other. From the theoretical point of view, the gapless feature is explained by the disorder-induced density of states in the nodal paired spinons (71, 80), whereas the gapped feature may be a consequence of the gapped spinless excitations (called visons), which are considerably greater than the bosonic spinon excitations (74). The latter may show a power law, as observed in $1/T_1$, in the quantum critical case (74). At present, we cannot assess the experiments and theories. Many ongoing studies are expected to provide significant information.

3. $Pd(dmit)_2$ COMPOUNDS

3.1. Crystal and Electronic Structures of $Pd(dmit)_2$ Compounds

The metal dithiolene complex $Pd(dmit)_2$ is an acceptor molecule and provides a number of conducting anion radical salts with monovalent cations, $Et_xMe_{4-x}Z^+$ (Et = C_2H_5-, Me = CH_3-, Z = N, P, As, Sb; x = 0, 1, 2) (11). Metal dithiolene complexes are planar π-conjugated molecules similar to tetrathiafulvalene (TTF) derivatives including ET. However, the carbon-carbon double bond in the central core of the TTF skeleton is replaced by the transition metal ion, which leads to a unique feature of frontier molecular orbitals. The metal d orbital has a very small overlap with the ligand orbitals in the HOMO owing to its symmetry (**Figure 10**). Lack of the metal-ligand interaction raises the HOMO energy level; thus, the HOMO-LUMO (lowest unoccupied molecular orbital) energy gap Δ is reduced, which is an important characteristic of metal dithiolene molecules (83, 84). The Δ value for $Pd(dmit)_2$ was estimated to be 0.8–0.9 eV by optical studies, whereas $\Delta \sim 3$ eV for ET (85). It should be noted that the symmetry of HOMO in $Pd(dmit)_2$ is similar to that in ET.

The $Pd(dmit)_2$ salts, (Cation) $[Pd(dmit)_2]_2$, exhibit two-dimensional layer structures that can be classified into the following types:

1. Single-layer structure (Cation = Et_2Me_2N, $EtMe_3N$): A unit cell contains one anion layer (86).
2. Solid crossing column structure: A unit cell contains two anion layers with different stacking directions of $Pd(dmit)_2$ units.
   a) α-type (Cation = Me_4N): Anion layers are crystallographically nonequivalent, and the anions show a corrugated arrangement along the interlayer direction (87).
   b) β-type (Cation = Me_4N): Anion layers are crystallographically equivalent, and the anions show a corrugated arrangement different from that in the α-type (87, 88).
   c) β'-type [Cation = Me_4Z (Z = P, As, Sb), Et_2Me_2Z (Z = P, As, Sb), $EtMe_3Z$ (Z = As, Sb)]: Very similar to β-type, but cation positions are slightly different (87, 89, 90).

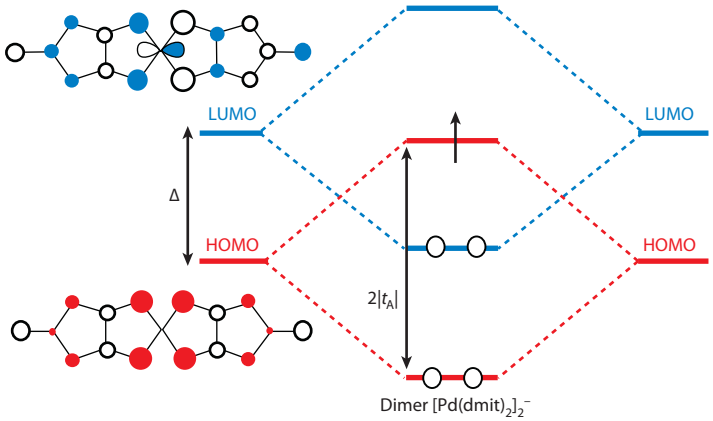

Figure 10

HOMO and LUMO of a $Pd(dmit)_2$ molecule and schematic electronic structure for a dimer unit $[Pd(dmit)_2]_2^-$. Abbreviations: HOMO, highest occupied molecular orbital; LUMO, lowest unoccupied molecular orbital.

d) γ-type (Cation = Me_4N): Anion layers are crystallographically equivalent, and the anions show a corrugated arrangement similar to that in the α-type (A. Nakao, A. Tajima & R. Kato, unpublished data).

3. Parallel column structure [Cation = $EtMe_3N$, $EtMe_3P$ (monoclinic and triclinic forms)]: A unit cell contains two anion layers and all the anion columns are parallel to each other (90).

They have the following common features:

1. $Pd(dmit)_2$ units are strongly dimerized with an eclipsed overlapping mode to form a dimer $[Pd(dmit)_2]_2^-$ with one negative charge. The degree of dimerization is stronger than that in the κ-type ET salts.
2. In contrast to the κ-type ET salts, the dimer units show face-to-face stacking.
3. Within the two-dimensional conduction layer, the dimer units form a quasi-triangular lattice.

Despite the above-mentioned common features, systematic discussion based on tunable parameters (for example, the frustration parameter t'/t, as shown later) can be possible only within the same structural type. Depending on the structural type, various low-temperature phases have been reported. Among them, the β- and β′-types and the $EtMe_3P$ salt (monoclinic) with the parallel column structure are well studied. The β-Me_4N salt with antiferromagnetic long-range order is the first pressure-induced superconductor of the $Pd(dmit)_2$ salts with closed-shell counter cations (91). It was revealed first in the β′-type salts that the frustration plays an important role in the $Pd(dmit)_2$ salts (92). The $EtMe_3P$ salt (monoclinic form) shows a second-order transition toward a VBS state with a spin gap where the lattice distortion forms pairs of the dimer units and the valence bond (the singlet pair) is formed between the dimer units (93). Under pressure, this VBS state turns to a superconducting state (90). This is the first example of the VBS state neighboring the superconducting phase (94–96). However, the $EtMe_3P$ salt (triclinic form) shows another type of VBS state coupled with the intradimer charge ordering (T. Yamamoto, Y. Nakazawa, M. Tamura, A. Nakao, A. Fukaya, R. Kato & K. Yakushi, to be submitted).

In this review, we focus on the β′-type salts where the crystal system is monoclinic and the space group is *C*2/*c* (**Figure 11**). The unit cell contains two crystallographically equivalent conduction layers (Layer 1 and Layer 2) interrelated by a glide plane. They are separated from each other by the insulating cation layer. Because the cations are located on the twofold axis,

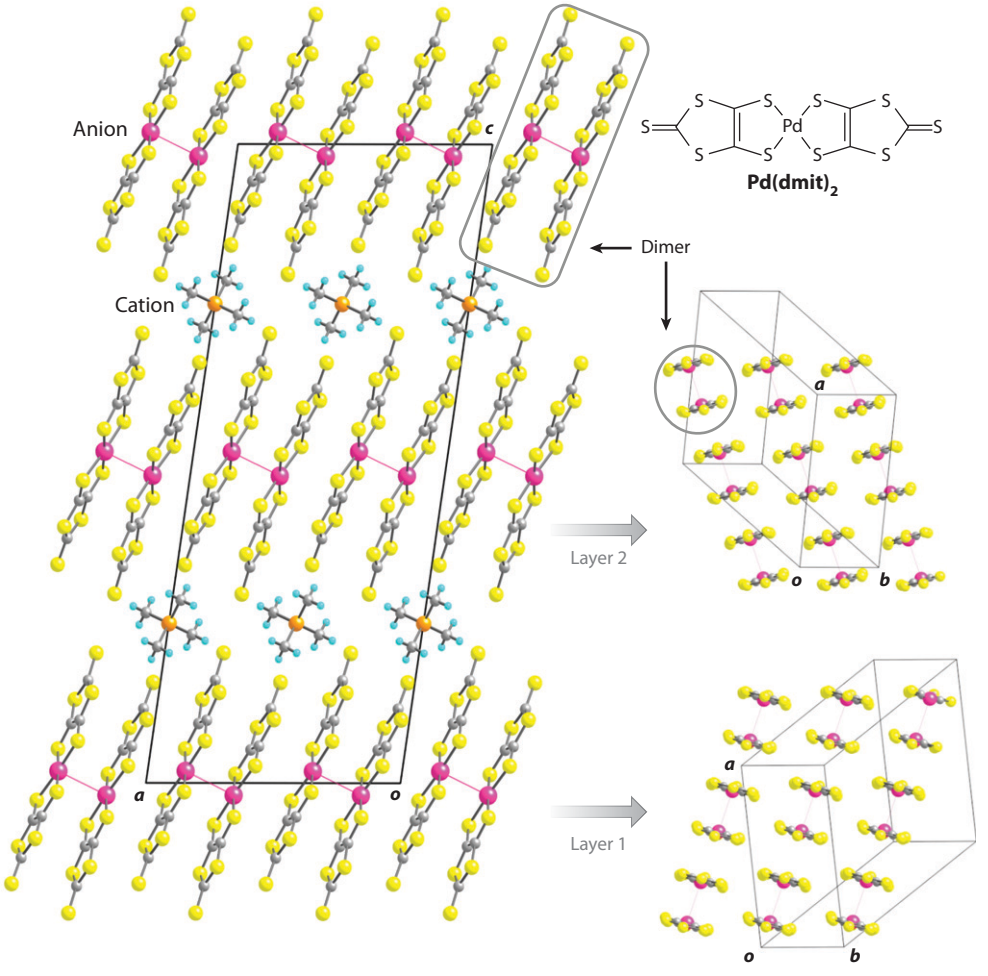

Figure 11

Crystal structure of the β′-type $Pd(dmit)_2$ salt.

the cation without the twofold symmetry ($EtMe_3Z^+$) shows two possible orientations with an occupancy of 50% for each one. The dimer units stack along the $a+b$ direction in Layer 1 and along the $a-b$ direction in Layer 2.

The strong dimerization and the small Δ value lead to an interesting electronic structure that has never been observed in other molecular conductors including the ET salts. In the dimer unit, each HOMO and LUMO in the monomer forms bonding and antibonding pairs with a dimerization gap (**Figure 10**). The dimerization gap is expressed as $2|t_A|$, where t_A is an intradimer transfer integral (**Figure 12**) and depends on the strength of dimerization. Both pairs have nearly the same t_A value. A transfer integral between the HOMO and LUMO is zero, because a difference in symmetry leads to cancellation of an overlap integral in an eclipsed overlapping mode. In the $Pd(dmit)_2$ salts, the dimerization gap is large enough, and the bonding LUMO pair is located below the antibonding HOMO pair. This is HOMO-LUMO level crossing (85, 97). The antibonding HOMO pair in $[Pd(dmit)_2]_2^-$ is occupied by one unpaired electron. In a crystal, each energy level forms an energy band, and the antibonding HOMO pair forms

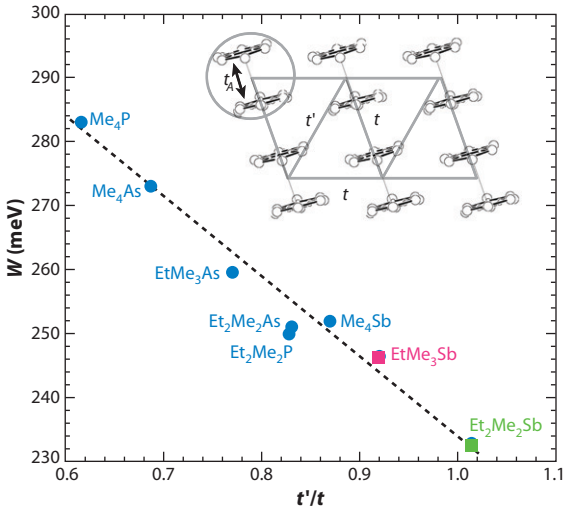

Figure 12

Relation between bandwidth (W) and frustration parameter (t'/t) in the β′-type Pd(dmit)$_2$ salts.

a half-filled two-dimensional conduction band. This means that the conduction band in the Pd(dmit)$_2$ salts originates from HOMO in a monomer, in contrast to the conventional acceptor-based molecular conductors. Because the conduction band is narrow and half-filled, the β′-Pd(dmit)$_2$ salts are Mott insulators at ambient pressure. The HOMO-LUMO level crossing plays an important role in the charge order transition, as described below.

The electronic structure around the Fermi level can be described by the dimer-based tight-binding approximation. In this model, the on-site Coulomb energy is read as effective Coulomb repulsive energy between carriers on a dimer (U_{eff}), which is enhanced by dimerization. Intermolecular HOMO···HOMO transfer integrals can be estimated from the extended Hückel molecular orbital calculation based on crystal structure data. Although the intermolecular Coulomb repulsion V in a dimer behaves as U_{eff} when the dimer is regarded as a single site, the intradimer transfer integral t_{A} can be used as a measure of U_{eff}, owing to local linearity of t_{A} and V versus a parameter that characterizes the dimeric structure (98). To be precise, the dimers form a scalene-triangular lattice where they are connected by three unequal transfer integrals. A dimer lattice of the $[\mathrm{Pd(dmit)_2}]_2^-$ units, however, is close to an isosceles-triangular lattice in many cases; thus, we treat it as an isosceles-triangular lattice with two transfer integrals t and t' in this review (**Figure 12**). The larger interdimer transfer integral t determines the bandwidth W. The ratio t_{A}/W roughly indicates the strength of the correlation effect in this Mott system. And, the ratio t'/t indicates deviation from the regular-triangular lattice (anisotropy) and thus the degree of frustration. These two parameters, t_{A}/W and t'/t, play important roles in understanding the electronic state in this Mott system (11). Interdimer transfer integrals (t, t') can be tuned by the choice of the cation. Depending on the cation, t'/t changes together with the bandwidth systematically (**Figure 12**). That is, as the system becomes anisotropic, the system has a wider conduction band.

3.2. Spin Liquid in Pd(dmit)$_2$ Compounds

In the Mott-insulating state, one spin is localized on each dimer. In the high-temperature region, the β′-Pd(dmit)$_2$ salts show frustrated paramagnetism that can be described by the model of

a spin-1/2 Heisenberg antiferromagnet on the triangular lattice (92). With decreasing temperature, the salts with large deviation from the regular triangular lattice undergo a transition toward antiferromagnetic long-range order and remove the spin frustration (**Figure 13**). In this thermal phase transition, an effect of frustration on the spin dynamics can be observed in μSR spectra (99). The Néel temperature decreases as the lattice gets close to the regular triangular lattice ($t'/t = 1.0$). In the region where the system has a nearly regular-triangular lattice ($t'/t \sim 1.0$) and the frustration strongly operates, the system shows various ground states instead of the antiferromagnetic long-range order (100). As for the β′-Pd(dmit)$_2$ salts, $EtMe_3Sb$ ($t'/t = 0.92$) and Et_2Me_2Sb ($t'/t = 1.01$) salts are situated in this region (**Figure 12**).

The Et_2Me_2Sb salt undergoes a first-order transition toward a nonmagnetic state (**Figure 13**) (101). Low-temperature X-ray crystal structure analysis and reflectivity spectra revealed that this is a charge order transition ($2[\text{dimer}]^- \rightarrow [\text{dimer}]^0 + [\text{dimer}]^{2-}$), which is accompanied by significant structural changes. Below the transition temperature, there exist two crystallographically independent dimers with different interplanar distances (102, 103). The neutral dimer shows stronger dimerization (shortened interplanar distance), whereas the divalent dimer shows weaker dimerization (elongated interplanar distance). The charge ordering transition in the Et_2Me_2Sb salt is associated with the HOMO-LUMO level crossing (**Figure 13**). The dimerization gap is enhanced in the neutral dimer with stronger dimerization. Because the bonding pairs are fully occupied and the antibonding pairs are vacant, the transition leads to the energy gain in the neutral dimer. However, the divalent dimer, where the antibonding pair is fully occupied, has the disadvantage of the bonding energy. But, the weaker dimerization that reduces the dimerization gap absorbs this energy cost. In the Et_2Me_2Sb salt, total gain of the bonding energy outweighs the energy cost of the lattice distortion. It should be emphasized that the HOMO-LUMO level crossing is indispensable to this mechanism (intradimer valence bond formation).

However, the $EtMe_3Sb$ salt shows a quantum spin liquid state (104). The static magnetic susceptibility shows frustrated paramagnetism that can be modeled by a spin-1/2 Heisenberg antiferromagnet on the triangular lattice with $J = 220$–250 K. There is no indication of the long-rang magnetic order down to 5 K (**Figure 13**). ^{13}C NMR spectra for the selectively

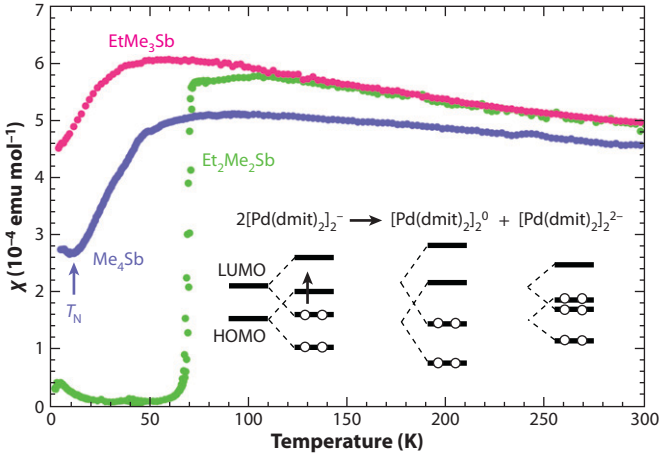

Figure 13

Temperature dependence of static magnetic susceptibility for Me_4Sb, $EtMe_3Sb$, and Et_2Me_2Sb salts. Abbreviations: HOMO, highest occupied molecular orbital; LUMO, lowest unoccupied molecular orbital.

enriched sample under 7.65 T do not show significant broadening down to 19.4 mK (**Figure 14*a***) (105). Although very slight gradual broadening is observed, the width is much smaller than the scale of the hyperfine coupling constant of the ^{13}C sites. This clearly indicates that there is no spin ordering or freezing down to the lowest temperature. Because this temperature is smaller than 0.01% of J, thermal fluctuations are completely negligible, and the absence of spin ordering or freezing should be attributed to quantum fluctuations.

The spin-lattice relaxation rate $1/T_1$ curve was fitted by the stretched exponential function. The stretching exponent β indicates homogeneity of the system. The β value being smaller than unity means that the system is inhomogeneous. The temperature dependence of β indicates that inhomogeneity is enhanced from approximately 20 K and reaches maximum around 1 K (**Figure 14*b*** inset). A sharp drop of $1/T_1$ below 1 K (**Figure 14*b***) strongly suggests a continuous phase transition that involves symmetry breaking and/or topological ordering (105). Below 1 K, the relaxation curves recover the homogeneous single-exponential nature, which is contradictory to the case of κ-$(ET)_2Cu_2(CN)_3$. In this region, $1/T_1$ is proportional to the square of the temperature. This is not the nature of the gapless spin liquid with the spinon Fermi surface, and this suggests a spin gap formation in the low temperature phase. Because the temperature dependence of $1/T_1$ obeys not an exponential law but a power law, the spin gap may be nodal, similar to that of anisotropic superconductivity.

However, heat capacity shows a different aspect (106). Compared with the Et_2Me_2Sb salt, which shows a nonmagnetic charge-ordered state with an excitation gap, the $EtMe_3Sb$ salt gives large absolute values of heat capacity (**Figure 15**). The most important point is that the $EtMe_3Sb$ salt shows a T-linear term in the zero-temperature limit, which means that the excitation from the ground state is gapless. Another important point is that the broad hump structure

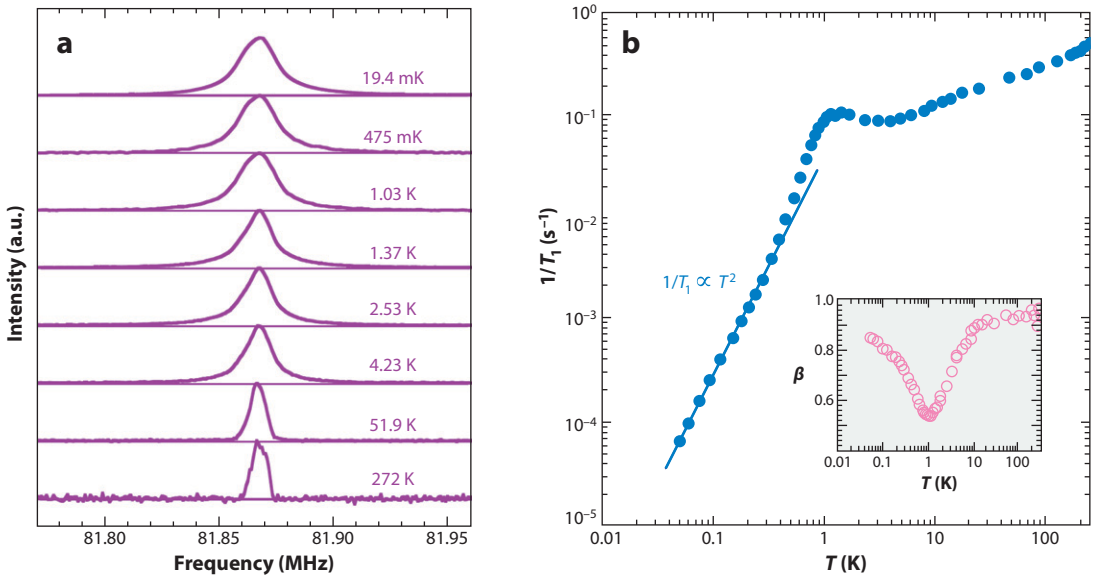

Figure 14

^{13}C NMR for randomly oriented samples of $EtMe_3Sb$ salt. (*a*) ^{13}C NMR spectra from 272 K to 19.4 mK. (*b*) Temperature dependence of ^{13}C nuclear spin-lattice relaxation rate ($1/T_1$). The relaxation of the nuclear magnetization $M(t)$ was analyzed using the stretched exponential function $1 - M(t)/M(\infty) = \exp\{-(t/T_1)^{\beta}\}$. The inset shows temperature dependence of the stretching exponent (β). Abbreviation: NMR, nuclear magnetic resonance.

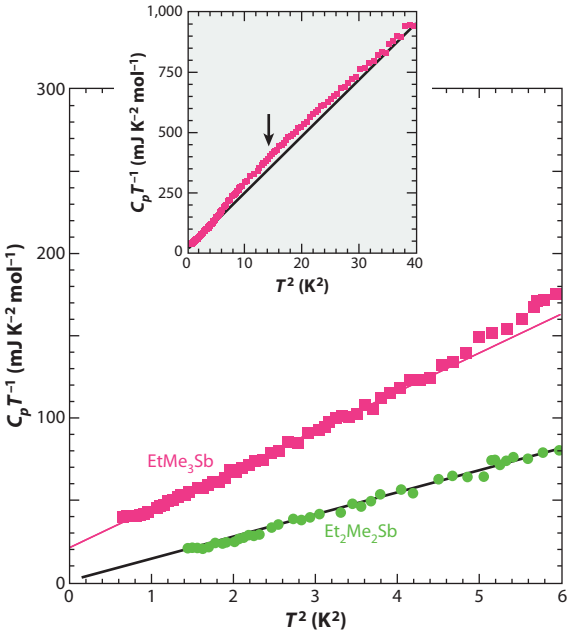

Figure 15

Low-temperature heat capacity (C_p) for $EtMe_3Sb$ and Et_2Me_2Sb salts. The main graph shows $C_p\ T^{-1}$ versus T^2 plots of the heat capacity. The inset shows a $C_p\ T^{-1}$ versus T^2 plot around a broad hump structure for the $EtMe_3Sb$ salt.

is observed around 3 K. This corresponds to the kink of $1/T_1$ in ^{13}C NMR in the same temperature region, and indicates a possibility of crossover phenomena to the spin liquid state.

Figure 16*a* shows temperature dependence of thermal conductivity (107). Compared with the Et_2Me_2Sb salt, the $EtMe_3Sb$ salt shows enhanced thermal conductivity, which indicates that spin-mediated contribution is added to the phonon contribution. Temperature dependence of the thermal conductivity has a peak structure around 1 K (**Figure 16*a*** inset). Thermal conductivity of the $EtMe_3Sb$ salt also shows a *T*-linear term, indicating gapless excitation from the ground state. This is markedly different from the case of κ-$(ET)_2Cu_2(CN)_3$.

Field dependence of thermal conductivity of the $EtMe_3Sb$ salt, however, suggests another kind of excitation (**Figure 16*b***). A steep increase above approximately 2 T is observed below 1 K, which implies that some spin-gap-like excitations are present at low temperatures, along with the gapless excitations indicated by the *T*-linear term. At present, there are two possible scenarios:

1. In terms of coexistence of the gapless and gapped excitations (108), the magnetic excitations are separated from the ground state by a spin gap, which is filled with nonmagnetic excitations.
2. In terms of a possible nodal gap structure in the spinon Fermi surface, the spin-gap-like behavior is attributed to the pairing gap formation, and the finite residual *T*-linear term stems from the zero-energy density of states similar to the disorder-induced normal fluid in d-wave superconductors (72).

Although there remain many open questions, the unusual bipartite nature of elementary excitations in the quantum spin liquid state places the $EtMe_3Sb$ salt in a key position for understanding Mott physics and quantum magnetism.

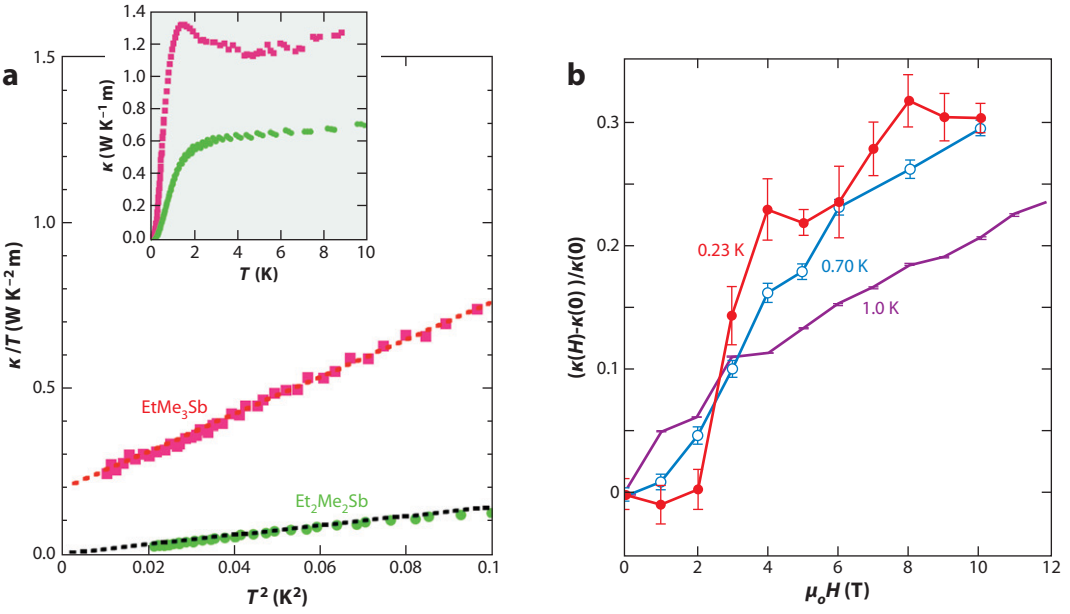

Figure 16

Low-temperature thermal conductivity (κ) for $EtMe_3Sb$ and Et_2Me_2Sb salts. (*a*) The main graph shows κ/T versus T^2 plots of the thermal conductivity. The inset shows temperature dependence of κ below 10 K in zero field. (*b*) Field dependence of thermal conductivity normalized by the zero-field value. The heat current was applied within the two-dimensional plane, and the magnetic field (H) was perpendicular to the plane.

Finally, it should be mentioned that one can easily obtain mixed crystals (alloys) in an isostructural series: $(EtMe_3Sb)_x(Et_2Me_2Sb)_{1-x}[Pd(dmit)_2]_2$. This provides a powerful experimental tuning knob of the interdimer transfer integrals. By increasing the $EtMe_3Sb$ content (x), the t'/t value decreases continuously, and the charge order transition temperature drops rapidly (T. Fukunaga, Y. Ishii, A. Tajima & R. Kato, unpublished data). As a consequence, we can summarize a general phase diagram for the β′-type $Pd(dmit)_2$ salts, as shown in **Figure 17**.

4. CONCLUSION

Mott transition was one of the most drastic correlation-induced phenomena proposed more than a half century ago. Theoretically, it came to be understood as a thermodynamic phase transition of scalar nature without symmetry breaking, as with the liquid-gas transition. Nevertheless, the critical phenomena, which are the fundamentals of phase transition, had been unexplored experimentally before the twenty-first century. The first experiment was for V_2O_3, a three-dimensional system with a critical temperature of 450 K, and indicated the criticality as expected in the liquid-gas transition; that is, the Ising universality class. The experiment on the quasi-two-dimensional system, κ-$(ET)_2Cu[N(CN)_2]Cl$, described in this review, is the second. However, the resultant criticality is different from that of V_2O_3. The unconventional criticality is possibly a consequence of quantum nature, which comes into Mott transition with a low critical temperature, as in the present case ($T_c = 40$ K); although, this is not fully agreed upon. Moreover, the observation of Mott criticality in both spin and charge channels behaving oppositely but with an identical exponent demonstrates that the order parameter is the density of spinless charge carriers.

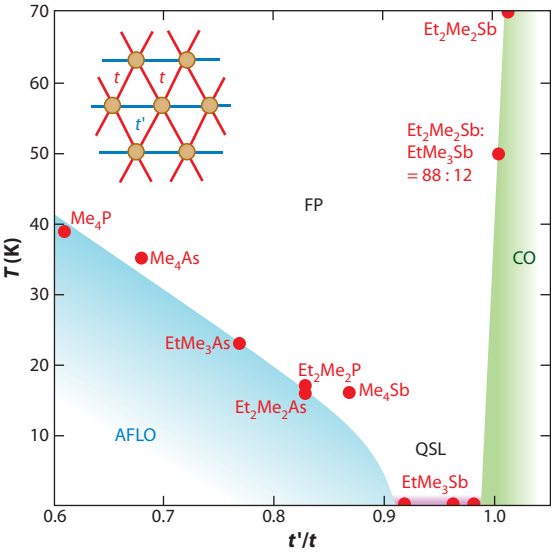

Figure 17

Phase diagram for the β′-Pd(dmit)$_2$ salts. Abbreviations: FP, frustrated paramagnetic (state); AFLO, antiferromagnetic long-range ordered (state); CO, charge-ordered (state); QSL, quantum spin liquid (state).

The issue of spin frustration has long been a central subject in the study of magnetism. In particular, the possible spin liquid on triangular lattices has been of keen interest as a novel quantum phase of matter and has become increasingly attractive with the idea that this state is possibly behind high-T_c superconductivity (109). However, the triangular-lattice Heisenberg model was found to have the 120-degree-oriented Néel ground state instead of any quantum-disordered state (54). In such a situation, however, it is found that spin states without magnetic ordering, which should be called spin liquid, were found in the two organic Mott insulators, κ-$(ET)_2Cu_2(CN)_3$ and $EtMe_3Sb[Pd(dmit)_2]_2$, which reside near the Mott transition. With the use of chemical/physical pressure and intense theoretical works, the series of experiments showed that the spin liquid is realized in a range of anisotropy of triangular lattices and in the intermediately correlated regime on the verge of Mott transition, not in the strongly correlated regime; namely, the electron itinerancy in the Mott insulator is key to realizing spin liquid on quasi-triangular lattices. How the spin liquid connects to the metallic and superconducting phases is a problem to consider in the future.

The nature of spin liquid in the two materials is mysterious. The excitation gap in κ-$(ET)_2Cu_2(CN)_3$ is controversial; specific heat points to a gapless ground state, whereas thermal conductivity behaves as though gapped by 0.46 K. The NMR relaxation rate exhibits a power-law temperature dependence, which is in between the two extreme behaviors. As for $EtMe_3Sb[Pd(dmit)_2]_2$, both thermodynamic measurements are consistent with gapless excitations, while the NMR relaxation rate may suggest a nodal gap. The result of thermal conductivity showing a *T*-linear term with a long mean-free path of μm will strongly constrain theoretical models. Appearance of anomalies at finite temperatures can be a signature of some kind of symmetry breaking. In this sense, the 5–6 K anomaly observed in NMR, specific heat, and thermal conductivity in κ-$(ET)_2Cu_2(CN)_3$ points to this possibility. Interestingly, 1 K is the characteristic temperature in the NMR relaxation rate for both materials, whereas it is not so

clear thermodynamically. As far as the present results are concerned, we guess that there is a variation in the nature of spin liquid, which is dependent on detailed material characteristics.

With organic materials such as model systems of strongly correlated electrons, we have reached a stage where the criticality of the Mott transition is experimentally assessed. Moreover, we have obtained the long-anticipated quantum spin liquid, which has just begun to be studied.

DISCLOSURE STATEMENT

The authors are not aware of any affiliations, memberships, funding, or financial holdings that might be perceived as affecting the objectivity of this review.

ACKNOWLEDGMENTS

We thank the following colleagues for their contribution to the works presented here: K. Miyagawa, Y. Shimizu, F. Kagawa, T. Itou, Y. Kurosaki, H. Kasahara, H. Hashiba, T. Furukawa, M. Maesato, G. Saito, Y. Nakazawa, S. Yamashita, A. Kawamoto, M. Tamura, A. Tajima, N. Tajima, H.M. Yamamoto, K. Kubo, Y. Ishii, A. Nakao, A. Fukaya, T. Fukunaga, T. Yamamoto, M. Yamashita, Y. Matsuda. We also thank H. Fukuyama, T. Senthil, M. Imada, P.A. Lee, S. Sachdev, J. Schmalian, S. Mazumdar, T. Mori, M. Ogata, and N. Nagaosa for stimulating discussion. K.K. is thankful for hospitalities in the following programs: Correlated Behavior and Quantum Criticality in Heavy Fermion and Related Systems at Aspen Center for Physics, The Physics of Higher Temperature Superconductivity at KITP of UCSB, and Pressure Effects on Materials at ICMR of UCSB. This work is partially supported by MEXT Grant-in-Aids for Scientific Research on Innovative Area (New Frontier of Materials Science Opened by Molecular Degrees of Freedom; no. 20110002), JSPS Grant-in-Aids for Scientific Research (A) (no. 20244055), and MEXT Global COE Program at University of Tokyo (Global Center of Excellence for the Physical Sciences Frontier; no. G04).

LITERATURE CITED

1. Ishiguro T, Yamaji K, Saito G. 1998. *Organic Superconductors*. New York: Springer
2. **2009. *Chem. Rev.* 104(11):4887–5782.**
3. Lebed A, ed. 2008. *The Physics of Organic Superconductors and Conductors*. New York: Springer. 754 pp
4. Mott NF. 1990. *Metal-Insulator Transitions*. London: Taylor & Francis. 278 pp.
5. Imada M, Fujimori A, Tokura Y. 1998. *Rev. Mod. Phys.* 70:1039–263
6. Anderson PW. 1973. *Mater. Res. Bull.* 8:153–60
7. Lee PA. 2008. *Science* 321:1306–7
8. Balents L. 2010. *Nature* 464:199–208
9. Sachdev S. 2008. *Nat. Phys.* 4:173–85
10. Kanoda K. 2006. *J. Phys. Soc. Jpn.* 75:051007
11. Kato R. 2004. *Chem. Rev.* 104:5319–46
12. Mori T. 1999. *Bull. Chem. Soc. Jpn.* 72:179–97
13. Castellani C. 1979. *Phys. Rev. Lett.* 43:1957–60
14. Georges A, Kotliar G, Krauth W, Rozenberg MJ. 1996. *Rev. Mod. Phys.* 68:13–125
15. Kotliar G, Lange E, Rozenberg MJ. 2000. *Phys. Rev. Lett.* 84:5180–83
16. Kawamoto A, Miyagawa K, Nakazawa Y, Kanoda K. 1995. *Phys. Rev. Lett.* 74:3455–58
17. Kawamoto A, Miyagawa K, Nakazawa Y, Kanoda K. 1995. *Phys. Rev. B* 52:15522–33

2. Features recent physical and chemical research on the molecular conductors

18. Kino H, Fukuyama H. 1995. *J. Phys. Soc. Jpn.* 64:2726–29
19. Kanoda K. 1997. *Hyperfine Interact.* 104:235–49
20. Kanoda K. 1997. *Physica C* 287:299–302
21. McKenzie R. 1997. *Science* 278:820–21
22. Miyagawa K, Kanoda K, Kawamoto A. 2004. *Chem. Rev.* 104:5635–53
23. Miyagawa K, Kawamoto A, Kanoda K. 2002. *Phys. Rev. Lett.* 89:017003
24. Kurosaki Y, Shimiza Y, Miyagawa K, Kanoda K, Saito G. 2005. *Phys. Rev. Lett.* 95:177001
25. Miyagawa K, Kawamoto A, Nakazawa Y, Kanoda K. 1995. *Phys. Rev. Lett.* 75:1174–77
26. Kandpal HC, Opahle I, Zhang Y-Z, Jeschke HO, Valenti R. 2009. *Phys. Rev. Lett.* 103:067004
27. Ito H, Ishiguro T, Kubota M, Saito G. 1996. *J. Phys. Soc. Jpn.* 65:2987–93
28. Limelette P, Wzietek P, Florens S, Georges A, Costi TA, et al. 2003. *Phys. Rev. Lett.* 91:016401
29. Kagawa F, Itou T, Miyagawa K, Kanoda K. 2004. *Phys. Rev. B* 69:064511
30. Kagawa F, Itou T, Miyagawa K, Kanoda K. 2004. *Phys. Rev. Lett.* 93:127001
31. Lefebvre S, Wzietek P, Brown S, Bourbonnais C, Jérome D, et al. 2000. *Phys. Rev. Lett.* 85:5420–23
32. Founier D, Poirier M, Castonguay M, Truong KD. 2003. *Phys. Rev. Lett.* 90:127002
33. Hassan SR, Georges A, Krishnamurthy HR. 2005. *Phys. Rev. Lett.* 94:036402
34. Souza M, Brühl A, Strack Ch, Wolf B, Schweitzer D, Lang M. 2007. *Phys. Rev. Lett.* 99:037003
35. Ohashi T, Momoi T, Tsunetsugu H, Kawakami N. 2008. *Phys. Rev. Lett.* 100:076402
36. Park H, Haule K, Kotliar G. 2008. *Phys. Rev. Lett.* 101:186403
37. Liebsch A, Ishida H, Merino J. 2009. *Phys. Rev. B* 79:195108
38. Kagawa F, Miyagawa K, Kanoda K. 2005. *Nature* 436:534–37
39. Georges A. 2004. *AIP Conf. Proc.* 715:3–74
40. Onoda S, Imada M. 2003. *Phys. Rev. B* 67:161102
41. Limelette P, Georges A, Jérome D, Wzietek P, Metcalf P, Honig JM. 2003. *Science* 302:89–92
42. Kadanoff LP, Gotze W, Hamblen D, Hecht R, Lewis EAS, et al. 1967. *Rev. Mod. Phys.* 39:395–431
43. Kagawa F, Miyagawa K, Kanoda K. 2009. *Nat. Phys.* 5:880–84
44. Imada M. 2003. *Phys. Rev. B* 72:075113
45. Misawa T, Imada M. 2007. *Phys. Rev. B* 75:115121
46. Papanikolaou S, Fernandes RM, Fradkin E, Phillips PW. 2008. *Phys. Rev. Lett.* 100:026408
47. Bartosch L, de Souza M, Lang M. 2010. Scaling theory of the Mott transition and breakdown of Grüneisen scaling near a finite-temperature critical end point. arXiv.1004.4898v1
48. Komatsu T, Matsukawa N, Inoue T, Saito G. 1996. *J. Phys. Soc. Jpn.* 65:1340–54
49. Nakamura K, Yoshimoto Y, Kosugi T, Arita R, Imada M. 2009. *J. Phys. Soc. Jpn.* 78:083710
50. Shimizu Y, Miyagawa K, Kanoda K, Maesato M, Saito G. 2003. *Phys. Rev. Lett.* 91:107001
51. Zheng W, Singh RRP, McKenzie RH, Coldea R. 2005. *Phys. Rev. B* 71:134422
52. Miyagawa K, Kawamoto A, Uchida K, Kanoda K. 2000. *Physica B* 284-288:1589–90
53. Smith DF, De Soto SM, Slichter CP, Schlueter JA, Kini AM, Daugherty RG. 2003. *Phys. Rev. B* 68: 024512
54. Huse DA, Elser V. 1988. *Phys. Rev. Lett.* 60:2531–34
55. Morita H, Watanabe S, Imada M. 2002. *J. Phys. Soc. Jpn.* 71:2109–12
56. Mizusaki T, Imada M. 2006. *Phys. Rev. B* 74:014421
57. Singh A. 2005. *Phys. Rev. B* 71:214406
58. Liu J, Schmalian J, Trivedi N. 2005. *Phys. Rev. Lett.* 94:127003
59. Kyung B, Tremblay A-MS. 2006. *Phys. Rev. Lett.* 97:046402
60. Sahebsara P, Senechal D. 2006. *Phys. Rev. Lett.* 97:257004
61. Powell BJ, McKenzie RH. 2007. *Phys. Rev. Lett.* 98:027005
62. Koretsune T, Motome Y, Furusaki A. 2007. *J. Phys. Soc. Jpn.* 76:074719
63. Clay RT, Li H, Mazumdar S. 2008. *Phys. Rev. Lett.* 101:166403
64. Watanabe T, Yokoyama H, Tanaka Y, Inoue J. 2008. *Phys. Rev. B* 77:214505
65. Tocchio LF, Parola A, Gros C, Becca F. 2009. *Phys. Rev. B* 80:064419
66. Yoshioka T, Koga A, Kawakami N. 2009. *Phys. Rev. Lett.* 103:036401
67. Baskaran G. 1989. *Phys. Rev. Lett.* 63:2524–27

68. LiMing W, Misguich G, Sindzingre P, Lhuillier C. 2000. *Phys. Rev. B* 62:6372–77
69. Motrunich OI. 2005. *Phys. Rev. B* 72:045105
70. Lee S-S, Lee PA. 2005. *Phys. Rev. Lett.* 95:036403
71. Grover T, Trivedi N, Senthil T, Lee PA. 2010. *Phys. Rev. B* 81:245121
72. Alicea J, Motrunich OI, Fisher MPA. 2006. *Phys. Rev. B* 73:174430
73. Raman KS, Moessner R, Sondhi SL. 2005. *Phys. Rev. B* 72:064413
74. Qi Y, Xu C, Sachdev S. 2009. *Phys. Rev. Lett.* 102:176401
75. Xu C, Sachdev S. 2009. *Phys. Rev. B* 79:064405
76. Shimizu Y, Miyagawa K, Kanoda K, Maesato M, Saito G. 2006. *Phys. Rev. B* 73:140407
77. Yamashita S, Nakazawa Y, Oguni M, Oshima Y, Nojiri H, et al. 2008. *Nat. Phys.* 4:459–62
78. Yamashita M, Nakata N, Kasahara Y, Sasaki T, Yoneyama N, et al. 2009. *Nat. Phys.* 5:44–47
79. Manna RS, de Souza M, Bruhl A, Schlueter JA, Lang M. 2010. *Phys. Rev. Lett.* 104:016403
80. Lee S-S, Lee PA, Senthil T. 2007. *Phys. Rev. Lett.* 98:067006
81. Galitski V, Kim YB. 2007. *Phys. Rev. Lett.* 99:266403
82. Kawamura H, Miyashita S. 1984. *J. Phys. Soc. Jpn.* 53:4138–54
83. Canadell E. 1997. *N. J. Chem.* 21:1147–59
84. Miyazaki T, Ohno T. 1999. *Phys. Rev. B* 59:R5269–72
85. Tajima H, Naito T, Tamura M, Kobayashi A, Kuroda H, et al. 1991. *Solid State Commun.* 79:337–41
86. Kobayashi H, Bun K, Naito T, Kato R, Kobayashi A. 1992. *Chem. Lett.* 21:1909–12
87. Kobayashi A, Kim H, Sasaki Y, Murata K, Kato R, Kobayashi H. 1990. *J. Chem. Soc. Faraday Trans.* 86:361–69
88. Kobayashi A, Miyamoto A, Kato R, Sato A, Kobayashi H. 1998. *Bull. Chem. Soc. Jpn.* 71:997–1006
89. Kato R, Liu Y-L, Hosokoshi Y, Aonuma S, Sawa H. 1997. *Mol. Cryst. Liq. Cryst.* 296:217–44
90. Kato R, Tajima A, Nakao A, Tamura M. 2006. *J. Am. Chem. Soc.* 128:10016–17
91. Kobayashi A, Kobayashi H, Miyamoto A, Kato R, Clark RA, Underhill AE. 1991. *Chem. Lett.* 20:2163–66
92. Tamura M, Kato R. 2002. *J. Phys. Condens. Matter* 14:L729–34
93. Tamura M, Nakao A, Kato R. 2006. *J. Phys. Soc. Jpn.* 75:093701
94. Shimizu Y, Akimoto H, Tsujii H, Tajima A, Kato R. 2007. *Phys. Rev. Lett.* 99:256403
95. Ishii Y, Tamura M, Kato R. 2007. *J. Phys. Soc. Jpn.* 76:033704
96. Itou T, Oyamada A, Maegawa S, Kubo K, Yamamoto HM, Kato R. 2009. *Phys. Rev. B* 79: 174517
97. Canadell E, Ravy S, Pouget JP, Brossard L. 1990. *Solid State Commun.* 75:633–38
98. Tamura M, Kato R. 2004. *J. Phys. Soc. Jpn.* 73:3108–10
99. Ohira S, Tamura M, Kato R, Watanabe I, Iwasaki M. 2004. *Phys. Rev. B* 70: 220404(R)
100. Tamura M, Kato R. 2009. *Sci. Technol. Adv. Mater.* 10:024304
101. Tamura M, Kato R. 2004. *Chem. Phys. Lett.* 387:448–52
102. Nakao A, Kato R. 2005. *J. Phys. Soc. Jpn.* 74:2754–63
103. Tamura M, Takenaka K, Takagi H, Sugai S, Tajima A, Kato R. 2005. *Chem. Phys. Lett.* 411:133–37
104. Itou T, Oyamada A, Maegawa S, Tamura M, Kato R. 2008. *Phys. Rev. B* 77:104413
105. Itou T, Oyamada A, Maegawa S, Kato R. 2010. *Nat. Phys.* 6:673–76
106. Yamashita S. 2010. *Thermodynamic study of quantum spin liquid behaviors in organic Mott insulators with triangular lattice structure*. PhD thesis. Osaka Univ., Osaka
107. Yamashita M, Nakata N, Senshu Y, Nagata M, Yamamoto HM, et al. 2010. *Science* 328:1246–48
108. Waldtmann C, Everts H-U, Bernu B, Lhuillier C, Sindzingre P, et al. 1998. *Eur. Phys. J. B* 2:501–7
109. Lee PA, Nagaosa N, Wen X-G. 2006. *Rev. Mod. Phys.* 78:17–85

Annual Review of Condensed Matter Physics

Volume 2, 2011

Contents

Errata

An online log of corrections to *Annual Review of Condensed Matter Physics* articles may be found at http://conmatphys.annualreviews.org/errata.shtml